Monthly Notices of the ROYAL ASTRONOMICAL SOCIETY

MNRAS **522,** 3188–3200 (2023) https://doi.org/10.1093/mnras/stad1175
Advance Access publication 2023 April 20

Late-formed haloes prefer to host quiescent central galaxies – I. Observational results

Kai Wang [1★] Yangyao Chen [2,3] Qingyang Li [4,5,6] and Xiaohu Yang [4,5,7,8]

[1] *Kavli Institute for Astronomy and Astrophysics, Peking University, Beijing 100871, China*
[2] *School of Astronomy and Space Science, University of Science and Technology of China, Hefei, Anhui 230026, China*
[3] *Key Laboratory for Research in Galaxies and Cosmology, Department of Astronomy, University of Science and Technology of China, Hefei, Anhui 230026, China*
[4] *Department of Astronomy, School of Physics and Astronomy, Shanghai Jiao Tong University, Shanghai 200240, China*
[5] *Shanghai Key Laboratory for Particle Physics and Cosmology, Shanghai Jiao Tong University, Shanghai 200240, China*
[6] *Institute for Astronomy, University of Edinburgh, Royal Observatory, Edinburgh EH9 3HJ, UK*
[7] *Tsung-Dao Lee Institute, Shanghai Jiao Tong University, Shanghai 200240, China*
[8] *Key Laboratory for Particle Physics, Astrophysics and Cosmology, Ministry of Education, Shanghai Jiao Tong University, Shanghai 200240, China*

Accepted 2023 April 14. Received 2023 March 23; in original form 2023 January 21

ABSTRACT

The star formation and quenching of central galaxies are regulated by the assembly histories of their host haloes. In this work, we use the central stellar mass to halo mass ratio as a proxy of halo formation time, and we devise three different models, from the physical hydrodynamical simulation to the empirical statistical model, to demonstrate its robustness. With this proxy, we inferred the dependence of the central galaxy properties on the formation time of their host haloes using the SDSS main galaxy sample, where central galaxies are identified with the halo-based group finder. We found that central galaxies living in late-formed haloes have higher quiescent fractions and lower spiral fractions than their early-formed counterparts by $\lesssim 8$ per cent . Finally, we demonstrate that the group finding algorithm has a negligible impact on our results.

Key words: methods: statistical – galaxies: groups: general – dark matter – large-scale structure of Universe.

1 INTRODUCTION

In the concordance ΛCDM model, the basic blocks of the cosmic structure are dark matter haloes, the virialized parts of the cosmic density field assembled through gravitational instability. The abundance, spatial distribution, and formation histories of the dark matter halo population are now well understood using semi-analytical methods and numerical simulations (e.g. Mo & White 1996; Navarro, Frenk & White 1997; Jing 2000; Wechsler et al. 2002; Gao, Springel & White 2005; Mo, Van den Bosch & White 2010; Chen et al. 2020). This provides a solid foundation to understand the galaxy population, as galaxies are believed to form and evolve in dark matter haloes and the properties of galaxies are expected to be closely related to their host haloes (White & Rees 1978).

Many methods have been used to establish the connection between galaxies and dark matter haloes in the framework provided by current cosmology. These include direct numerical simulations that are based on the first principles of physical processes combined with some subgrid recipes for modelling unresolved processes (e.g. Vogelsberger et al. 2013; Schaye et al. 2015; Davé, Thompson & Hopkins 2016; Weinberger et al. 2017; Davé et al. 2019; Nelson et al. 2019), semi-analytical models that are based on a set of empirical functions to approximate physical processes of galaxy formation and evolution (e.g. White & Frenk 1991; Kauffmann, White & Guiderdoni 1993; Somerville & Primack 1999; Cole et al. 2000; Kang et al. 2005; Guo et al. 2011; Henriques et al. 2015), and empirical models that aim to establish the connection between galaxies and haloes statistically and empirically (e.g. Jing, Mo & Börner 1998; Berlind et al. 2003; Yang, Mo & van den Bosch 2003; Kravtsov et al. 2004; Vale & Ostriker 2004; Zheng et al. 2005; Moster, Naab & White 2013; Lu et al. 2014; Behroozi et al. 2019). A primary consensus on the galaxy–halo connection has been reached that the stellar mass–halo mass relation is non-linear but is roughly described by a double-power-law function (Yang et al. 2003; Behroozi, Wechsler & Conroy 2013; Wechsler & Tinker 2018). Such a relation has been used to indicate that the efficiency of converting baryons into stars is suppressed in both the low-mass and high-mass ends, respectively, by supernova feedback (e.g. Dekel & Silk 1986; Ceverino & Klypin 2009) and active galactic nuclei (AGNs) feedback (e.g. Croton et al. 2006; Fabian 2012), although the details remain uncertain.

Motivated by the success in establishing the primary connection between galaxies and dark matter haloes, attempts have been made to extend the galaxy–halo connection using other (secondary) properties of galaxies and haloes. An important example is the attempt to relate the assembly histories of haloes to the star formation histories of galaxies using heuristic assumptions that are tuned to match the observed abundance and spatial distribution of galaxies as a function of their secondary properties, such as colour and star formation rate (SFR; e.g. Hearin & Watson 2013; Hearin et al. 2014; Watson et al. 2015; Moster, Naab & White 2018; Behroozi

★ E-mail: wkcosmology@gmail.com

et al. 2019; Meng et al. 2020; Wang et al. 2023b). Hydrodynamical simulations were also used to investigate the secondary effects in the galaxy–halo connection. For example, Davies et al. (2020) found that central galaxies living in early-formed haloes tend to possess fewer amounts of gas in the circumgalactic medium (CGM), harbour more massive black holes, have longer cooling time for the CGM gas, and, consequently, are more quenched in star formation. Such correlations indicate that early-formed haloes tend to host central galaxies that are more quiescent (see also Matthee & Schaye 2019). The causality between halo formation and star formation status is further confirmed by Davies, Crain & Pontzen (2021) using a controlled simulation that follows the details of halo formation and star formation. They found that early-formed haloes grow their central black holes earlier so that their feedback can quench the star formation activity earlier than that in late-formed counterparts. In contrast, Cui et al. (2021) found that early-formed haloes actually prefer to host star-forming central galaxies in their SIMBA simulation (Davé et al. 2016; Davé et al. 2019). They argued that central galaxies in early-formed haloes are able to accumulate a large amount of cold gas through cold-mode accretion at high-z (Birnboim & Dekel 2003; Kereš et al. 2005; van de Voort et al. 2011; Wright et al. 2021) and that the associated quasar-mode AGN feedback is inefficient to quench galaxies but can extend the star formation time-scale. On the other hand, late-formed haloes, which acquire their gas mainly through hot-mode accretion, host central galaxies with smaller amounts of cold gas, and the radio-mode AGN feedback associated with such accretion can quench these galaxies. This scenario seems to be supported by observational results where red central galaxies prefer to live in more massive haloes (which tend to form later) than their blue counterparts of the same stellar mass (e.g. Mandelbaum et al. 2006; More et al. 2011; Mandelbaum et al. 2016; Wechsler & Tinker 2018; Posti, Fraternali & Marasco 2019; Posti & Fall 2021; Zhang et al. 2022).

In order to study the impact of halo formation histories on central galaxies, it is crucial to fix the halo mass and find an observational quantity that can be used as a proxy of halo formation time. Wang et al. (2011) found that the mass ratio between the central subhalo and the host halo is strongly correlated with the formation time of the host halo. Motivated by this and the expectation that the stellar mass of a galaxy is correlated with the mass of its subhalo, Lim et al. (2016) suggested that the central stellar mass to halo mass ratio (hereafter central SMHMR) may be used as an observational proxy of halo formation time (see also Tojeiro et al. 2017; Bradshaw et al. 2020; Zhang, Yang & Guo 2021). In this paper, we adopt the same proxy and apply it to the observational data. We will show that central galaxies with lower SMHMRs are more quenched. To make connections to halo formation time, we calibrate the relation between central SMHMRs and halo formation time using three different models, and they all agree with each other. We then use this relation to quantify how the quenched fraction and the spiral fraction of galaxies depend on the formation time of their host haloes.

The paper is organized as follows. In Section 2, we describe the halo formation time proxy and derive its relationship with halo formation time using three different models, from the physical hydrodynamical simulation of IllustrisTNG to the empirical subhalo halo abundance-matching method. In Section 3, we apply the proxy on the observational data to study the dependence of central galaxy properties on the halo formation time. Finally, our results are summarized in Section 4. We converted all of the presented results to a concordance ΛCDM cosmology with $H_0 = 100h$ km s^{-1} Mpc^{-1}, $h = 0.7$, $\Omega_\Lambda = 0.75$, and $\Omega_m = 0.25$.

2 TESTING THE PROXY OF HALO FORMATION TIME

2.1 The proxy

Previous studies suggest that the central SMHMR is a proxy of the halo formation time, where haloes that are formed earlier prefer to host more massive central galaxies and vice versa (Wang et al. 2011; Lim et al. 2016; Tojeiro et al. 2017; Bradshaw et al. 2020; Correa & Schaye 2020). Their relationship can be explained by that early formed haloes have more time for their satellites to merge with central galaxies.

A robust scaling relation between the central SMHMR and the halo formation time needs to be built before we can use this proxy. To this end, we devised three different models to quantify this scaling relation, as well as their scatters. We start from a cosmological hydrodynamical simulation with main haloes identified where the halo mass is denoted as $M_{h,\rm sim}$. Each dark matter halo contains no less than one subhalo and each subhalo contains one galaxy with stellar mass assigned, which is denoted as $M_{*,\rm sim}$. Besides, each subhalo also has a $V_{\rm peak}$, which is the peak value of the maximum circular velocity along the evolution history of this subhalo. Then, we devised three models with different assignments of stellar mass and halo mass to subhaloes and haloes, i.e.

(i) `Model-A`: We use stellar mass and halo mass from the simulation, i.e. $M_{*,\rm sim}$ and $M_{h,\rm sim}$. The central galaxy is defined as the one with the largest $M_{*,\rm sim}$.

(ii) `Model-B`: We use stellar mass for each subhalo in the simulation, i.e. $M_{*,\rm sim}$, and recalibrate the halo mass for each main halo with the abundance-matching method according to the rank of the total stellar mass of member galaxies with $M_{*,\rm sim} \geq 10^9 {\rm M}_\odot$, and this halo mass is denoted as $M_{h,\rm AM}$. The central galaxy is defined as the one with the largest $M_{*,\rm sim}$.

(iii) `Model-C`: This model is fully empirical and independent of the specific implementation of baryonic physics. First, we assign stellar mass to each subhalo using the abundance-matching method according to the rank of $V_{\rm peak}$, and this stellar mass is denoted as $M_{*,\rm AM'}$ (Reddick et al. 2013). During the abundance-matching procedure, the observational stellar mass function in Moustakas et al. (2013) is adopted.[1] Then, we recalibrate the halo mass for each main halo with the abundance-matching method according to the rank of the sum of $M_{*,\rm AM'}$ for all member galaxies with $M_{*,\rm AM'} \geq 10^9 {\rm M}_\odot$, and this halo mass is denoted as $M_{h,\rm AM'}$. The central galaxy is defined as the one with the largest $M_{*,\rm AM'}$.

These notations are summarized in Table 1. We note that `Model-A` totally relies on the hydrodynamical simulation, so the stellar mass and halo mass are both physical but depend on the specific implementation of the simulation used. On the contrary, `Model-C` only relies on the heuristic assumption of abundance-matching. And `Model-B` is in between. Using these three models, from the physical hydrodynamical simulation to the empirical statistical model, we will demonstrate that they all agree on the scaling relation between the central SMHMR and the formation time of their host haloes, showing the robustness of this relation.

[1] We note that the stellar mass function measurement in Moustakas et al. (2013) suffers from systematic effects in photometry. To maintain consistency in observational data, we adopt the recalibrated results in Behroozi et al. (2019) where an attempt was made to deal with these issues.

Table 1. Notations used in this paper.

Notation	Description
$V_{\rm peak}$	Peak value of the maximum circular velocity of subhaloes along the main branch.
$t_{\rm form}$	Lookback time when the FoF halo has first assembled half of its final mass along the main branch
$\Delta t_{\rm form}$	Residual of $t_{\rm form}$ with respect to the median $t_{\rm form}$ in bins of halo mass
central SMHMR	The SMHMR for central galaxies
$M_{*,\rm sim}$	Stellar mass of galaxies/subhaloes in the hydrodynamical simulation
$M_{*,\rm AM'}$	Stellar mass assigned to each subhalo using the abundance-matching method according to the rank of $V_{\rm peak}$ based on the observational stellar mass function
$M_{h,\rm AM}$	Halo mass assigned to each FoF halo using the abundance-matching method according to the rank of the sum of $M_{*,\rm sim}$ for all subhaloes in this FoF halo
$M_{h,\rm AM'}$	Halo mass assigned to each FoF halo using the abundance-matching method according to the rank of the sum of $M_{*,\rm AM'}$ for all subhaloes in this FoF halo

2.2 Numerical simulations used for the test

Here we use the state-of-the-art simulation of IllustrisTNG to test the scaling relation between central SMHMRs and halo formation time. The IllustrisTNG [The Next Generation (TNG); Weinberger et al. 2017; Marinacci et al. 2018; Naiman et al. 2018; Nelson et al. 2018; Springel et al. 2018; Pillepich et al. 2018a,b; Nelson et al. 2019] is a suite of gravo-magnetohydrodynamical cosmological simulations run with the moving-mesh code AREPO. TNG simulates the formation and evolution of galaxies from $z = 127$ to $z = 0$ based on a cosmology consistent with results in Planck Collaboration (2016), where $\Omega_{\Lambda,0} = 0.6911$, $\Omega_{b,0} = 0.3089$, $\sigma_8 = 0.8159$, $n_s = 0.9667$, and $h = 0.6774$. Here we use TNG300-1 for better statistics, which has 2×2500^3 resolution elements in a box with the side length of $205h^{-1}$cMpc. The target baryon mass resolution is 1.1×10^7 M$_\odot$, and the dark matter particle mass is 5.9×10^7 M$_\odot$.

In the TNG simulation, dark matter haloes were identified with the friends-of-friends (FoF) algorithm using dark matter particles.[2] Substructures were identified with the SUBFIND algorithm (Springel et al. 2001) using all types of particles, where the baryonic components identified are defined as galaxies, with the dark matter components as subhaloes. The subhalo located at the minimum of the gravitational potential is defined as the central one, while others are satellites. Subhalo merger trees are built using the SUBLINK algorithm (Rodriguez-Gomez et al. 2015). Once all the trees are built up, we can define the main progenitor of any subhalo in the preceding snapshot as the one with *the most massive progenitor history* (see De Lucia & Blaizot 2007). Finally, we can obtain a branch consisting of the main progenitors of the halo in question by recursively identifying the main progenitor, and this branch is called the main branch.

The halo mass is defined as the total mass within a sphere around the halo centre where the mean overdensity is 200 times the critical density of the universe. The peak halo mass of a subhalo is defined as the maximum halo mass that the subhalo has ever achieved along the main branch when it is identified as a central subhalo. For each subhalo, we can also calculate its maximum circular velocity and denote it as $V_{\rm max}$. Then, we trace the main branch of this subhalo to find the peak value for all $V_{\rm max}$ on this branch and denote it as $V_{\rm peak}$.

The assembly history of each dark matter halo corresponds to a subhalo merger tree, where small haloes are formed early, then they merge with each other and end up with one descendant halo at $z = 0$. Despite the complexity of this merger tree, we can still capture the main feature with the characteristic formation time of haloes (Chen et al. 2020). There are many different definitions of halo formation time (e.g. Gao et al. 2005; Wechsler et al. 2006; Li, Mo & Gao 2008; Nadler et al. 2023), and here we choose to use the simplest one, which is defined as the highest redshift when the main progenitor halo has assembled half of its descendant halo mass at $z = 0$. The corresponding lookback time is denoted as $t_{\rm form}$.

[2]These haloes are also called main haloes or FoF haloes, and we will use them interchangeably.

2.3 Test results

2.3.1 *Comparison of three models*

We first examine the difference in halo masses for these three models. The left-hand panel in Fig. 1 shows the comparisons between $M_{h,\rm sim}$ and $M_{h,\rm AM}$. Here, the circles with error bars show the median and 16 per cent − 84 per cent quantiles, and the dashed line is the one-to-one reference line. Similarly, the middle panel shows the comparison between $M_{h,\rm sim}$ and $M_{h,\rm AM'}$. All these results show that the halo masses assigned according to the empirical abundance-matching method are very close to the values in the TNG300 simulation.

Then, we examine the relationship between three halo masses and halo formation time, $t_{\rm form}$, which is shown on the right-hand panel in Fig. 1. The symbols are the median $t_{\rm form}$ in each halo mass bin. The solid lines are the corresponding linear fitting line, while the black/blue/red colours are for three models accordingly. Here one can see that all three models produce a nearly identical negative correlation between halo mass and halo formation time, where massive haloes are formed late, which is expected in the hierarchical structure formation scenario. We note that this correlation can introduce bias into our study when a finite halo mass bin is used. Hence, we use the residual with respect to the median $t_{\rm form}$ as a function of halo mass, i.e.

$$\Delta t_{\rm form} = t_{\rm form} - \texttt{Median}\,(t_{\rm form}(M_h))\,. \quad (1)$$

Finally, to see if the abundance-matching method introduces any dependence on the halo formation time, we compare the halo mass in three models for early formed and late-formed haloes separately, where haloes with $\Delta t_{\rm form} > 0$ in each $M_{h,\rm sim}$ bin are defined as early formed and others are late-formed. The results are shown in the first three panels of Fig. 1 with magenta and cyan solid lines, respectively. Here one can see that our abundance-matching method does not introduce any obvious bias.

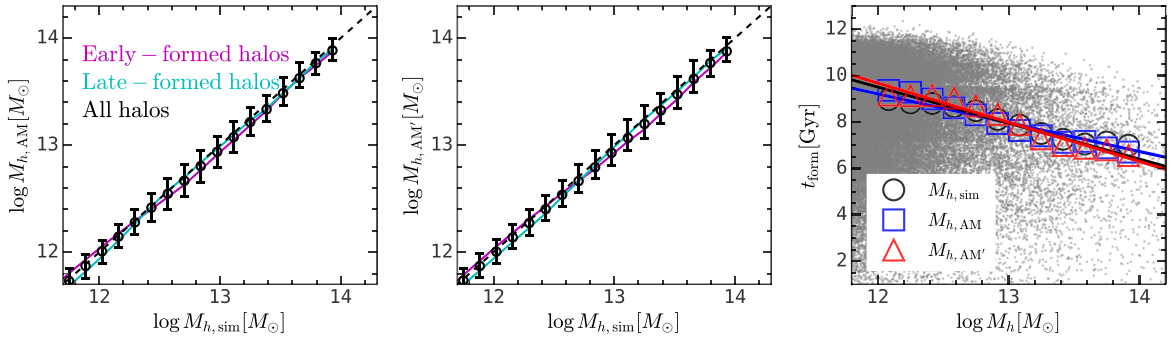

Figure 1. Left-hand panel: Comparison of halo mass between the TNG300 simulation, $M_{h,\mathrm{sim}}$, and the abundance-matching result, $M_{h,\mathrm{AM}}$, according to the rank of the sum of $M_{*,\mathrm{sim}}$ in each group. **Middle panel:** Comparison of halo mass between the TNG300 simulation, $M_{h,\mathrm{sim}}$, and the abundance-matching result, $M_{h,\mathrm{AM'}}$, according to the rank of the sum of $M_{*,\mathrm{AM'}}$ in each group. In both panels, circles with error bars show the median value in each mass bin with errors estimated using the bootstrap method. The dashed line is the one-to-one reference line. Magenta and cyan lines are for early formed and late-formed haloes, respectively. **Right-hand panel:** Relation between halo mass and halo formation time. The background points are the TNG haloes. The black/blue/red symbols are for $M_{h,\mathrm{sim}}/M_{h,\mathrm{AM}}/M_{h,\mathrm{AM'}}$, respectively. In this paper, we only use galaxies with stellar mass above 10^9 $\mathrm{M}_\odot$ in haloes with halo mass above 10^{12} $\mathrm{M}_\odot$ for each definition of stellar mass and halo mass.

2.3.2 The central SMHMR-halo formation time relation

Fig. 2 shows the mean Δt_{form} as a function of central SMHMRs, as well as the standard deviation. The top/middle/bottom panels show the results in `Model-A`/`Model-B`/`Model-C`. Here one can see that all three models predict very similar scaling relations that haloes with higher central SMHMR are formed earlier. These results indicate that the central SMHMR-halo formation time relation does not depend on the specific implementation of baryonic physics in hydrodynamical simulations. Instead, this correlation can be explained by the hierarchical structure formation scenario, where early formed haloes have more time for their central galaxies to merge with their satellites. We also fit the scaling relations between central SMHMRs and Δt_{form} with linear functions for `Model-B` and `Model-C`, and present them with blue and red lines, respectively.

Fig. 3 shows the median central SMHMR as a function of Δt_{form} in four halo mass bins for three models. The scaling relations in `Model-B` and `Model-C` are fitted with quadratic polynomials, which are shown in blue and red solid curves. Here one can see that all three models predict that early formed haloes have higher central SMHMRs and the scaling relations are similar, except for massive haloes in `Model-C`. The discrepancies between `Model-C` and `Model-B`/`Model-A` are attributed to the difference in their stellar mass functions, where TNG300 underestimated the amplitude of stellar mass functions due to its relatively low resolution (Pillepich et al. 2018b). We also checked the relation using the EAGLE simulation and presented the result in Appendix A, which agrees well with our results here.

It is noteworthy that our results on the positive correlation between halo formation time and SMHMRs are consistent with previous studies on galaxy assembly bias (e.g. Zentner, Hearin & van den Bosch 2014; Hearin et al. 2016; Mao, Zentner & Wechsler 2018; Wang et al. 2019; Zu et al. 2021), which is the dependence of the halo occupation of galaxies on secondary properties of dark matter haloes manifested in their spatial distributions. Zentner et al. (2019) found that high-concentration haloes prefer to host more luminous central galaxies compared with their low-concentration counterparts of the same halo mass through a comprehensive Bayesian analysis; a similar conclusion is obtained in Wang et al. (2022) by combining several spatial summary statistics. In this paper, we use the group-based statistic, i.e. SMHMR, and obtain consistent results based on three different models, supporting previous findings.

3 APPLICATIONS TO REAL DATA

In the previous section, we established the relationship between central SMHMRs and halo formation time using three different models, from the physical hydrodynamical simulation to the empirical statistical model. All these models produce similar results that haloes with higher central SMHMRs are formed earlier, and vice versa. These results illustrate that the relation between halo formation time and the central SMHMRs neither relies on the specific implementation of galaxy formation models nor specific subgrid recipes (see Appendix A). With these scaling relations, we can use the central SMHMR as a proxy of halo formation time and study its relation with central galaxy properties in our real Universe.

3.1 Observational data

Here we use the GALEX-SDSS-WISE Legacy Catalog (GSWLC; Salim et al. 2016; Salim, Boquien & Lee 2018), which is constructed from the Sloan Digital Sky Survey (SDSS) main galaxy sample (MGS; York et al. 2000; Blanton et al. 2005; Abazajian et al. 2009). The SDSS MGS is a magnitude-limited spectroscopic survey with $r < 17$ and covers ~ 8000 deg^2. The stellar mass and the SFR are estimated from the ultraviolet-optical-infrared bands photometry using the CIGALE code (Noll et al. 2009; Boquien et al. 2019) with the stellar library of Bruzual & Charlot (2003) and the initial mass function of Chabrier (2003). The left-hand panel of Fig. 4 shows the distribution of galaxies on the $M_* -$ SFR plane. We further separate galaxies into the star-forming and quiescent populations according to that whether the SFR is more than 1 dex below the star-forming main sequence (see Woo et al. 2013; Wang, Peng & Chen 2023a). The separation line is

$$\log\left(\frac{\mathrm{SFR}}{\mathrm{M}_\odot\ \mathrm{yr}^{-1}}\right) = 0.82 \times \log\left(\frac{M_*}{\mathrm{M}_\odot}\right) - 9.17, \quad (2)$$

and shown as the black dashed line on the left-hand panel of Fig. 4.

Based on the GSWLC catalog, we constructed a M_*-limited sample using the method in Wang et al. (2023a; see also Pozzetti et al. 2010). They are shown in red points on the right-hand panel of Fig. 4 where the black dashed line shows the minimal stellar mass we can probe at each redshift. We also weigh each galaxy with $1/V_{\mathrm{max}}$, where V_{max} is the volume between $z_{\mathrm{min}} = 0.02$ and z_{max}, which is

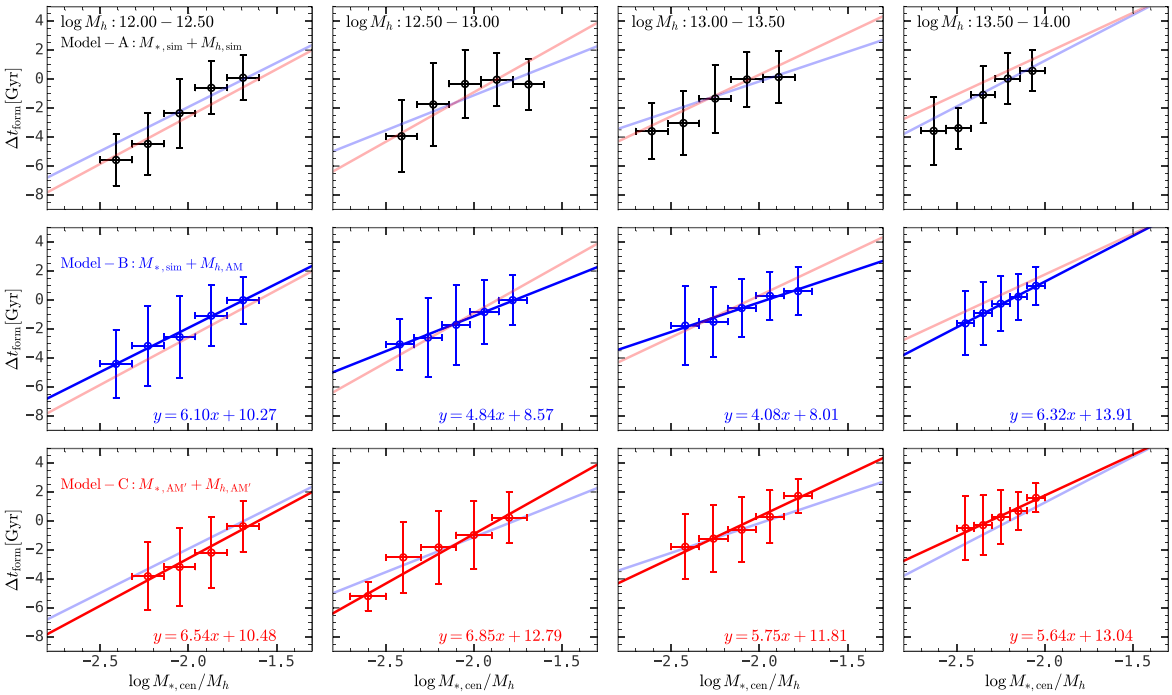

Figure 2. Relation between halo formation time, $\Delta t_{\rm form}$, and the central SMHMR, $\log(M_{*,\rm cen}/M_h)$. Symbols are the mean $\Delta t_{\rm form}$ in each central SMHMR bin with error bars showing the standard deviation. The blue/red solid lines are the linear fitting results for data points on the middle/bottom panels, respectively. **Top panels:** Both stellar mass and halo mass are from the TNG300 simulation, i.e. `Model-A`. **Middle panels:** The stellar mass is from the TNG300 simulation, and the halo mass is recalibrated by rank-matching the total stellar mass in each group, i.e. `Model-B`. **Bottom panels:** The stellar mass is recalibrated with the abundance-matching method according to the rank of $V_{\rm peak}$ for each subhalo, and the halo mass is recalibrated by rank-matching the total stellar mass in each group, i.e. `Model-C`. This figure illustrates that haloes with larger central SMHMRs are formed early.

inferred from the mass-limited envelope calculated above according to the stellar mass of each galaxy.

We use the morphology classification from the Galaxy Zoo project[3] (Lintott et al. 2011). Through Galaxy Zoo, galaxies are classified into different categories of morphology according to their visual image by citizen scientists, and each galaxy has more than 20 votes. Then a flag, i.e. `spiral`, `elliptical`, or `uncertain`, is assigned to each galaxy according to the note frequency corrected with a debiasing process (Bamford et al. 2009). Here we define spiral galaxies as those with the flag of `SPIRAL` set to unity.

We use the group catalog of Yang et al. (2007) to select central galaxies as the most massive one in each galaxy group. The halo mass is calibrated by abundance-matching the total stellar mass with theoretical halo mass function, where the stellar mass estimation is based on Bell et al. (2003). For the consistency of the stellar mass estimation, we recalibrate the halo mass for each group using the abundance-matching method, according to the rank of the sum of stellar mass estimated in Salim et al. (2016), which is

$$n_h\,(>M_h) = n_*\left(>M_{*,\rm tot}\right) \tag{3}$$

where the left-hand hand is the cumulative halo mass function and the right-hand hand is the cumulative total stellar mass function. The right-hand panel of Fig. 4 shows the comparison between the halo mass in Yang et al. (2007) and our recalibrated ones. In Appendix C, we demonstrated the importance of the halo mass recalibration to avoid bias, especially for low-mass groups.

[3]https://data.galaxyzoo.org/

3.2 The dependence of central galaxy properties on halo formation time

Fig. 5 shows the quiescent fraction and the spiral fraction of central galaxies as a function of central SMHMRs in four halo mass bins. As one can see, for the whole halo mass range, central galaxies with low SMHMRs are more quenched and have lower spiral fractions than those with high SMHMRs. The difference in the quiescent fraction ranges from ~ 10 per cent to $\gtrsim 20$ per cent, while the difference in the spiral fraction is about ~ 20 per cent across the whole halo mass range in question. It is noteworthy that we are using a broad halo mass bin width for better statistics. We also checked the results using finer halo mass bins in Appendix B, and the trend is consistent with the results shown here.

On the top x-axis of Fig. 5, we also show $\Delta t_{\rm form}$, which is converted from the central SMHMR using the scaling relation calibrated in `Model-C` (see bottom panels in Fig. 2). One can see that haloes with low central SMHMRs, which are formed late, are not only more quiescent but also have a lower fraction of spiral morphology. The range of the halo formation time we can probe is $\sim$4 Gyr in each halo mass bin. We note that the results in Fig. 5 cannot be simply interpreted as the dependence of the quiescent fraction and the spiral fraction on the halo formation time, because the scaling relation between $\Delta t_{\rm form}$ and the central SMHMR has a non-negligible scatter.

To derive the dependence of central galaxy properties on the formation time of their host haloes more strictly, we must consider the scatter in the scaling relation of central SMHMRs and halo formation time. To this end, we can express the distribution of

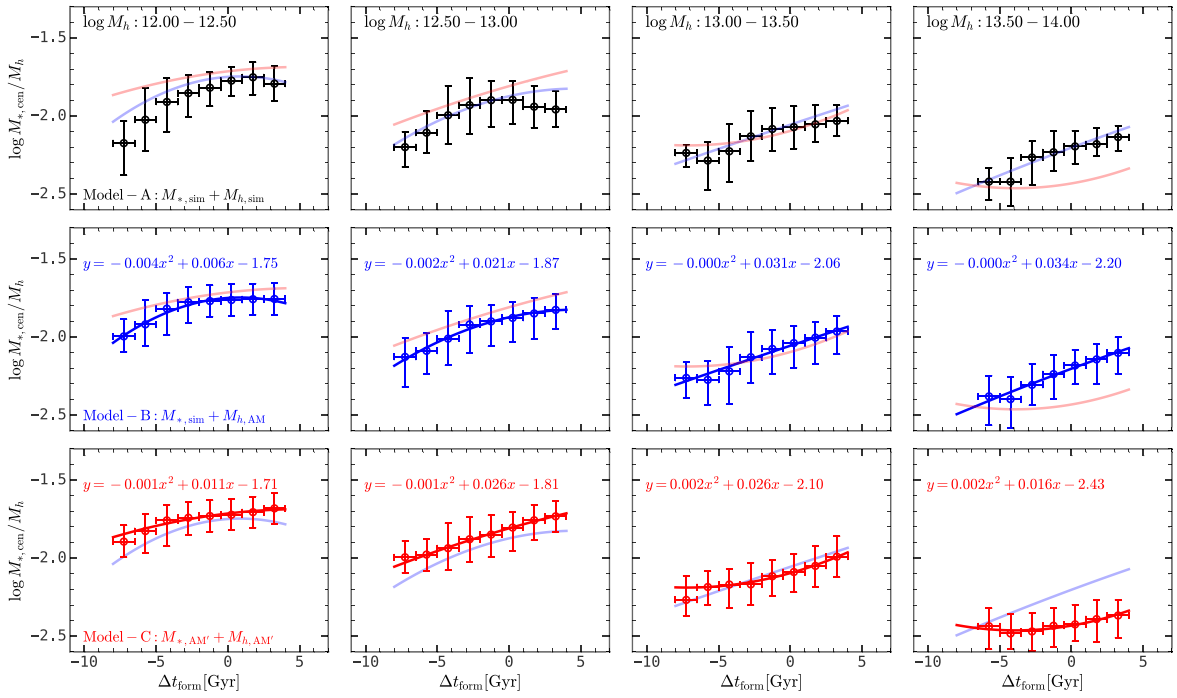

Figure 3. Relation between central SMHMR, $\log(M_{*,\rm cen}/M_h)$, and halo formation time, $\Delta t_{\rm form}$. Symbols are the median central SMHMR in each $\Delta t_{\rm form}$ bin with error bars showing the 16 per cent-84 per cent quantiles. The blue/red solid lines are the fitting results for data points on the middle/bottom panels, respectively. The stellar mass and halo mass for panels on different rows are the same as Fig. 2. This figure illustrates that early formed haloes tend to have larger central SMHMRs, i.e. more massive central galaxies.

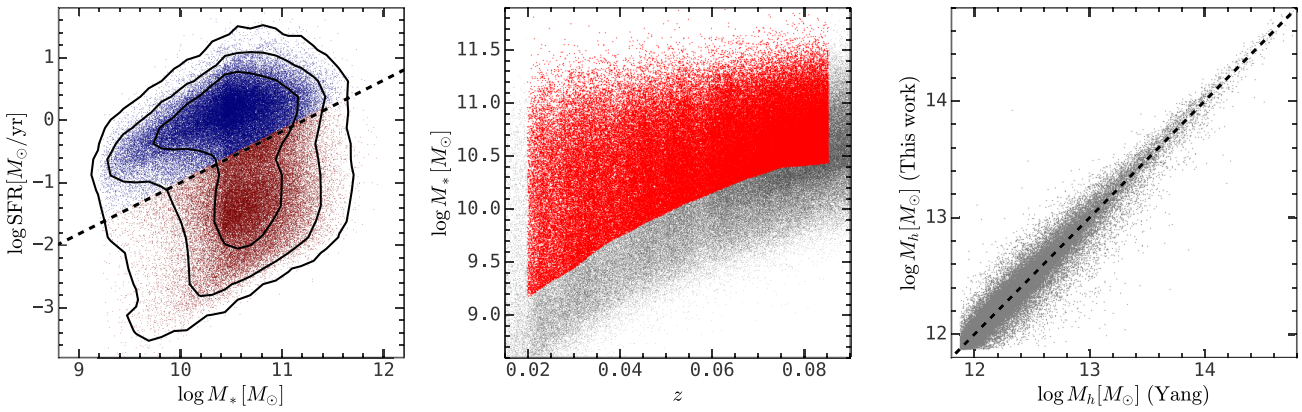

Figure 4. Left-hand panel: The distribution of galaxies on the stellar mass and SFR plane with black solid lines enclose 68 per cent, 95 per cent, and 99.7 per cent of the whole sample. The dashed line is the calibrated separation line for the star-forming and quiescent galaxies. The red points are quiescent galaxies and the blue ones are star-forming galaxies. **Middle panel:** The distribution of galaxies on the redshift and stellar mass plane, where red points are the selected mass-limited galaxies and grey points are the remaining ones. **Right-hand panel:** The comparison between the halo mass calibrated in Yang et al. (2007) and our recalibrated halo mass using the stellar mass from the GSWLC catalog [see equation (3)], and the black dashed line is the one-to-one reference line.

central galaxy properties, F, as a function of halo formation time, $\Delta t_{\rm form}$, as

$$\begin{aligned} P(F \mid \Delta t_{\rm form}) &= \int {\rm d}R P(F, R \mid \Delta t_{\rm form}) \\ &= \int {\rm d}R P(F \mid R, \Delta t_{\rm form}) P(R \mid \Delta t_{\rm form}) \\ &\approx \int {\rm d}R P(F \mid R) P(R \mid \Delta t_{\rm form}), \end{aligned} \tag{4}$$

where F represents the quiescent fraction or the spiral fraction, R is the central SMHMR, and $\Delta t_{\rm form}$ is the halo formation time defined in equation (1). We note that all of the probability distributions above are conditioned on halo mass, and we omit it for clarity. The final step of the above derivation is based on the assumption that $P(F|R, \Delta t_{\rm form}) \approx P(F|R)$, which assumes that the impact of the halo formation time on the star formation activities and morphologies of central galaxies is only through the central SMHMR.

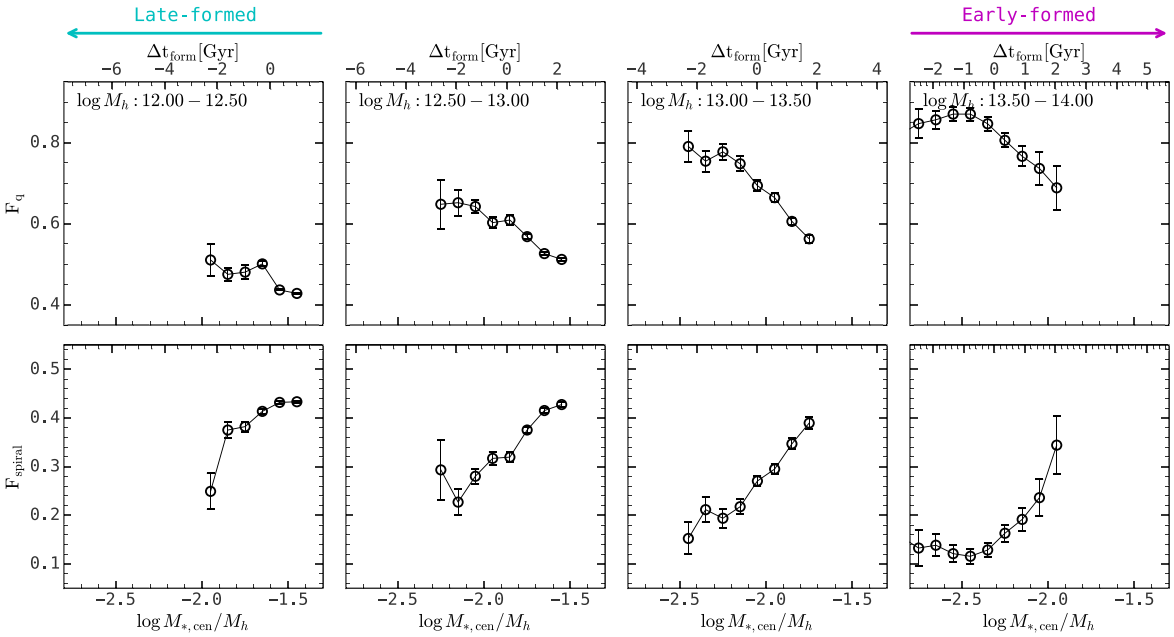

Figure 5. The quiescent fraction (**top panels**) and the spiral fraction (**bottom panels**) of central galaxies as a function of central SMHMRs in different halo mass bins. Error bars are estimated with the bootstrap method. The top x-axis shows the halo formation time converted from central SMHMRs using the scaling relation calibrated in `Model-C` (see bottom panels in Fig. 2). Haloes with larger $\Delta t_{\rm form}$ are formed earlier, as indicated by the arrows on the figure. This figure illustrates that central galaxies in haloes with high SMHMRs, which are formed early, have low quiescent fractions and higher spiral fractions.

Based on the above derivation, we can calculate the quiescent fraction and the spiral fraction of central galaxies as a function of the formation time of their host haloes. We start with all of the FoF haloes in the TNG300 simulation, where each halo has a halo mass and a central stellar mass assigned in `Model-B` (or `Model-C`), as well as a halo formation time, $\Delta t_{\rm form}$, calculated with equation (1). For each halo, we can calculate its central SMHMR, R, which is used to read a value of mean quiescent/spiral fraction $F(R)$ and the associated scatter $\sigma_F(R)$ from Fig. 5 in the corresponding halo mass bin. Then we generate a quiescent/spiral fraction for the halo in question from a normal distribution with a mean of $F(R)$ and a scatter of $\sigma_F(R)$. Finally, we can calculate the mean quiescent/spiral fraction for haloes with given halo masses and $\Delta t_{\rm form}$. The result is shown in Fig. 6, which shows the residual with respect to the mean quiescent/spiral fraction in each halo mass bin. The blue (red) symbols are results with `Model-B` (`Model-C`), where both models produce very similar results. Here one can see that central galaxies in late-formed haloes are more quiescent and have a lower fraction of spiral morphology than their early-formed counterparts. The difference in the quiescent fraction is about 2 per cent − 8 per cent for haloes with $M_h > 10^{12.5}$ M$_\odot$, and the difference in the spiral fraction is about 2 per cent − 8 per cent across the whole halo range in question.

The relation between halo formation time and central galaxy properties can also manifest itself as the difference in the formation time for haloes with star-forming/spiral and quiescent/non-spiral central galaxies. We present the result in Appendix C, which shows that haloes with star-forming/spiral central galaxies are formed earlier than their quiescent/non-spiral counterparts by $\lesssim$0.4 Gyr.

3.3 Impact of the group finding algorithm

Since dark matter haloes are difficult to be detected observationally, we rely on the group-finding algorithm to construct the group catalog (e.g. Eke et al. 2004; Yang et al. 2005; Berlind et al. 2006; Knobel et al. 2012; Wang et al. 2020). The performance of the halo-based group finder is tested in many previous studies (e.g. Yang et al. 2005, 2007; Lu et al. 2016; Lim et al. 2017; Yang et al. 2021), which shows that it can recover the input galaxy groups with high completeness and purity and calibrate the halo mass of galaxy groups to high accuracy, based on the mock test. Nevertheless, this group finder is poorly tested on the performance in recovering colour/SFR-related statistics (Campbell et al. 2015), like the quiescent fraction, which might jeopardize our conclusions in this paper. Here we want to examine if this contamination can bias our results. To this end, we applied the group-finding algorithm to a mock galaxy catalog and see whether the relation between central SMHMRs and quiescent fractions of central galaxies is biased.

The mock survey is constructed based on the N-body simulation of ELUCID (Wang et al. 2014, 2016), which is a constrained simulation with a box volume of (500 h^{-1}Mpc)^3 and 3072^3 dark matter particles. Dark matter haloes are identified with the FoF method and subhaloes are identified with the SUBFIND algorithm (Springel et al. 2001). The stellar mass and SFR are assigned to each subhalo according to the empirical model of MAHGIC, which is trained on the IllustrisTNG simulation (see Chen et al. 2021a,b, for more details). Here we only use galaxies with $M_* \geq 10^9$ M$_\odot$. The most massive galaxy in each FoF halo is defined as the central one, while others are satellites. The redshift-space position for each galaxy is generated using the method in Chen et al. (2019).

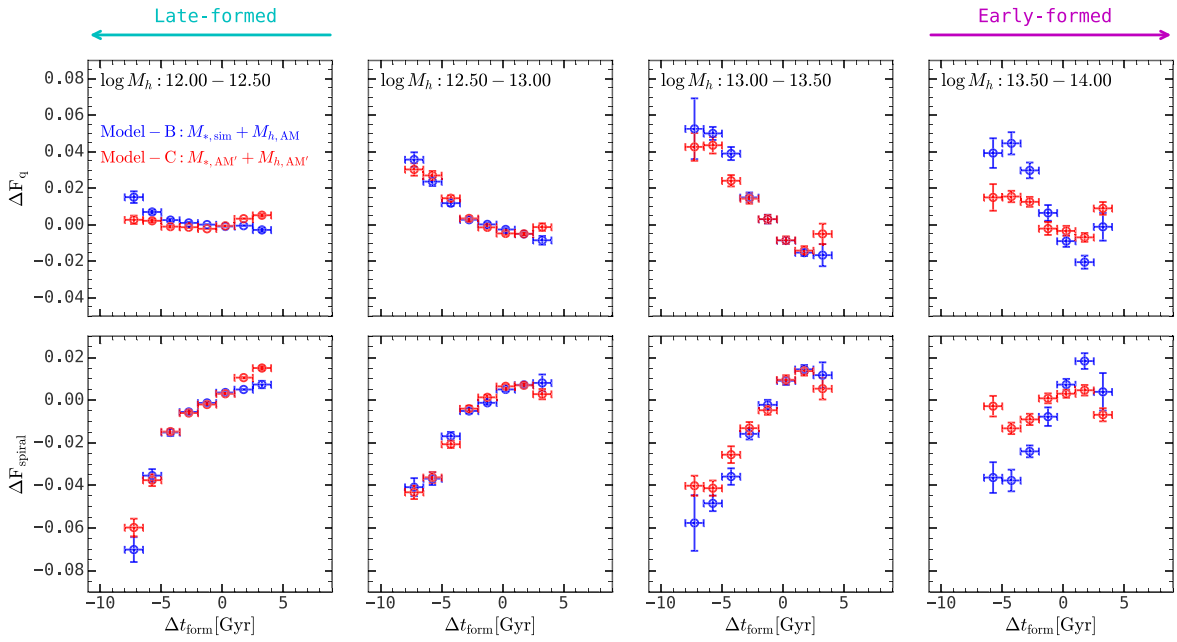

Figure 6. Dependence of the quiescent fraction and the spiral fraction on $\Delta t_{\rm form}$ derived from equation (4). Symbols show the mean deviation from the mean fraction in each halo mass bin with error bars estimated using the bootstrap method. This figure illustrates that central galaxies in late-formed haloes have higher quiescent fractions and lower spiral fractions.

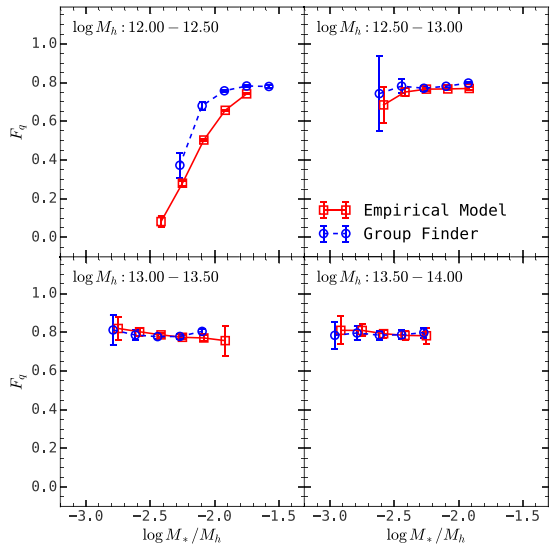

Figure 7. The quiescent fraction as a function of central SMHMRs in the empirical model of MAHGIC applied on the ELUCID simulation. The red colour shows the results of the input catalog. The blue colour shows the result of the halo-based group finder. Poisson errors are shown. This figure illustrates that the group-finding algorithm does not bias the dependence of the quiescent fraction of central galaxies on the central SMHMRs.

For each FoF halo in the mock volume, we re-assign its halo mass using the abundance-matching method according to the rank of the total stellar mass in this halo (see equation (3)). Then we calculate the fraction of quiescent galaxies, which is defined as those with SFR/$M_* < 10^{-11}\,{\rm yr}^{-1}$, as a function of central SMHMR in four halo mass bins. The results are shown in red squares in Fig. 7.

Then, we applied the halo-based group-finding algorithm in Yang et al. (2021) to these mock galaxies and constructed a galaxy group catalog (see also Lu et al. 2016; Lim et al. 2017; Yang et al. 2021; Li et al. 2022). For each identified galaxy group, the halo mass is assigned with the abundance-matching method according to the rank of the total stellar mass in each group, and the central galaxy is defined as the one with the largest stellar mass. Finally, we can plot the quiescent fraction as a function of central SMHMRs in four halo mass bins based on the identified galaxy group catalog, and the result is shown with blue circles in Fig. 7. As one can see, these two results are very similar to each other, indicating that the group-finding algorithm cannot bias this relation.

4 SUMMARY

It is generally believed that the star formation activities of galaxies are regulated by the formation histories of their host haloes. However, this correlation is difficult to be verified observationally for two reasons. First, the correlation between galaxy properties and the assembly histories of dark matter haloes is a secondary effect, while the primary correlation is the stellar mass-halo mass relation. Secondly, the halo formation histories are not observable, and finding a model-independent proxy is not trivial. In this paper, we devised three different models, from the physical hydrodynamical simulation to the empirical statistical model, to demonstrate the robustness of using the central SMHMR, i.e. central SMHMR, as a proxy of halo formation time. Then, we made use of the large galaxy sample from SDSS MGS, together with the physical quantities from the GSWLC catalog and the group catalog constructed by the halo-based group finder, to infer the relation between the central galaxy properties and the formation time of their host haloes. Our main results are summarized as follows:

(i) We established the relation between central SMHMRs and halo formation time, where early-formed haloes have higher central SMHMRs than their late-formed counterparts. This relation is tested on three models, from the physical hydrodynamical simulation to the empirical statistical model. All three models produce similar scaling relations, supporting the robustness of the central SMHMR as a halo formation time proxy. (see Figs 2 and 3).

(ii) Using the galaxy group catalog constructed on the SDSS MGS sample, we inferred the dependence of the central galaxy properties on the central SMHMRs. And we found that haloes with high SMHMRs have a higher fraction of star-forming/spiral central galaxies than their counterparts with low SMHMRs (see Fig. 5).

(iii) We derived the dependence of the quiescent fraction and the spiral fraction on the formation time of their host haloes. We found that central galaxies in late-formed haloes have higher fractions of quiescence and lower fractions of spiral morphology by $\lesssim 8$ per cent than their early-formed counterparts (see Fig. 6).

(iv) By applying the halo-based group-finding algorithm to a mock catalog, we found that it does not introduce any obvious bias into the relation between the quiescent fraction of central galaxies and the central SMHMRs (see Fig. 7).

Our results provide the first quantification of the relationship between central galaxy properties and the formation time of their haloes. This relationship can be further tested using alternative halo formation time proxies, like the stellar mass gap and the spatial distribution of satellite galaxies (Wechsler et al. 2002; Dariush et al. 2010; Farahi, Ho & Trac 2020; Golden-Marx et al. 2022). Meanwhile, these results can be compared with state-of-the-art hydrodynamical cosmological simulations, like IllustrisTNG (Pillepich et al. 2018a; Nelson et al. 2019), EAGLE (Schaye et al. 2015), and SIMBA (Davé et al. 2019), and test their different implementations of subgrid physics, which will be presented in the subsequent paper.

ACKNOWLEDGEMENTS

KW sincerely thanks Prof. Houjun Mo and Prof. Cheng Li for their helpful discussions. This work is supported by the National Science Foundation of China (NSFC) Grant No. 12125301, 12192220, and 12192222 and the science research grants from the China Manned Space Project with NO. CMS-CSST-2021- A07.

The authors acknowledge the Tsinghua Astrophysics High-Performance Computing platform at Tsinghua University for providing computational and data storage resources that have contributed to the research results reported within this paper.

Funding for the SDSS and SDSS-II has been provided by the Alfred P. Sloan Foundation, the Participating Institutions, the National Science Foundation, the U.S. Department of Energy, the National Aeronautics and Space Administration, the Japanese Monbukagakusho, the Max Planck Society, and the Higher Education Funding Council for England. The SDSS Web Site is http://www.sdss.org/.

The SDSS is managed by the Astrophysical Research Consortium for the Participating Institutions. The Participating Institutions are the American Museum of Natural History, Astrophysical Institute Potsdam, University of Basel, University of Cambridge, Case Western Reserve University, University of Chicago, Drexel University, Fermilab, the Institute for Advanced Study, the Japan Participation Group, Johns Hopkins University, the Joint Institute for Nuclear Astrophysics, the Kavli Institute for Particle Astrophysics and Cosmology, the Korean Scientist Group, the Chinese Academy of Sciences (LAMOST), Los Alamos National Laboratory, the Max-Planck-Institute for Astronomy (MPIA), the Max-Planck-Institute for Astrophysics (MPA), New Mexico State University, Ohio State University, University of Pittsburgh, University of Portsmouth, Princeton University, the United States Naval Observatory, and the University of Washington.

DATA AVAILABILITY

The data underlying this article will be shared on reasonable request to the corresponding author. The computation in this work is supported by the HPC toolkit **HIPP** at https://github.com/ChenYangyao/hipp.

REFERENCES

Abazajian K. N. et al., 2009, ApJS, 182, 543
Bamford S. P. et al., 2009, MNRAS, 393, 1324
Behroozi P. S., Wechsler R. H., Conroy C., 2013, ApJ, 770, 57
Behroozi P., Wechsler R. H., Hearin A. P., Conroy C., 2019, MNRAS, 488, 3143
Bell E. F., McIntosh D. H., Katz N., Weinberg M. D., 2003, ApJS, 149, 289
Berlind A. A. et al., 2003, ApJ, 593, 1
Berlind A. A. et al., 2006, ApJS, 167, 1
Birnboim Y., Dekel A., 2003, MNRAS, 345, 349
Blanton M. R. et al., 2005, AJ, 129, 2562
Boquien M., Burgarella D., Roehlly Y., Buat V., Ciesla L., Corre D., Inoue A. K., Salas H., 2019, A&A, 622, A103
Bradshaw C., Leauthaud A., Hearin A., Huang S., Behroozi P., 2020, MNRAS, 493, 337
Bruzual G., Charlot S., 2003, MNRAS, 344, 1000
Campbell D., van den Bosch F. C., Hearin A., Padmanabhan N., Berlind A., Mo H. J., Tinker J., Yang X., 2015, MNRAS, 452, 444
Ceverino D., Klypin A., 2009, ApJ, 695, 292
Chabrier G., 2003, PASP, 115, 763
Chen Y., Mo H. J., Li C., Wang H., Yang X., Zhou S., Zhang Y., 2019, ApJ, 872, 180
Chen Y., Mo H. J., Li C., Wang H., Yang X., Zhang Y., Wang K., 2020, ApJ, 899, 81
Chen Y., Mo H. J., Li C., Wang K., 2021a, MNRAS, 504, 4865
Chen Y., Mo H. J., Li C., Wang K., Wang H., Yang X., Zhang Y., Katz N., 2021b, MNRAS, 507, 2510
Cole S., Lacey C. G., Baugh C. M., Frenk C. S., 2000, MNRAS, 319, 168
Collaboration P. et al., 2014, A&A, 571, A1
Correa C. A., Schaye J., 2020, MNRAS, 499, 3578
Croton D. J. et al., 2006, MNRAS, 365, 11
Cui W., Davé R., Peacock J. A., Anglés-Alcázar D., Yang X., 2021, Nature Astron., 5, 1069
Dariush A. A., Raychaudhury S., Ponman T. J., Khosroshahi H. G., Benson A. J., Bower R. G., Pearce F., 2010, MNRAS, 405, 1873
Davé R., Thompson R., Hopkins P. F., 2016, MNRAS, 462, 3265
Davé R., Anglés-Alcázar D., Narayanan D., Li Q., Rafieferantsoa M. H., Appleby S., 2019, MNRAS, 486, 2827
Davies J. J., Crain R. A., Oppenheimer B. D., Schaye J., 2020, MNRAS, 491, 4462
Davies J. J., Crain R. A., Pontzen A., 2021, MNRAS, 501, 236
De Lucia G., Blaizot J., 2007, MNRAS, 375, 2
Dekel A., Silk J., 1986, ApJ, 303, 39
Eke V. R. et al., 2004, MNRAS, 348, 866
Fabian A. C., 2012, ARA&A, 50, 455
Farahi A., Ho M., Trac H., 2020, MNRAS, 493, 1361
Gao L., Springel V., White S. D. M., 2005, MNRAS, 363, L66
Golden-Marx J. B. et al., 2022, ApJ, 928, 28
Guo Q. et al., 2011, MNRAS, 413, 101
Hearin A. P., Watson D. F., 2013, MNRAS, 435, 1313
Hearin A. P., Watson D. F., Becker M. R., Reyes R., Berlind A. A., Zentner A. R., 2014, MNRAS, 444, 729

Hearin A. P., Zentner A. R., van den Bosch F. C., Campbell D., Tollerud E., 2016, MNRAS, 460, 2552
Henriques B. M. B., White S. D. M., Thomas P. A., Angulo R., Guo Q., Lemson G., Springel V., Overzier R., 2015, MNRAS, 451, 2663
Jing Y. P., 2000, ApJ, 535, 30
Jing Y. P., Mo H. J., Börner G., 1998, ApJ, 494, 1
Kang X., Jing Y. P., Mo H. J., Borner G., 2005, ApJ, 631, 21
Kauffmann G., White S. D. M., Guiderdoni B., 1993, MNRAS, 264, 201
Kereš D., Katz N., Weinberg D. H., Davé R., 2005, MNRAS, 363, 2
Knobel C. et al., 2012, ApJ, 753, 121
Kravtsov A. V., Berlind A. A., Wechsler R. H., Klypin A. A., Gottlöber S., Allgood B., Primack J. R., 2004, ApJ, 609, 35
Li Y., Mo H. J., Gao L., 2008, MNRAS, 389, 1419
Li Q. et al., 2022, ApJ, 933, 9
Lim S. H., Mo H. J., Wang H., Yang X., 2016, MNRAS, 455, 499
Lim S. H., Mo H. J., Lu Y., Wang H., Yang X., 2017, MNRAS, 470, 2982
Lintott C. et al., 2011, MNRAS, 410, 166
Lu Z., Mo H. J., Lu Y., Katz N., Weinberg M. D., van den Bosch F. C., Yang X., 2014, MNRAS, 439, 1294
Lu Y. et al., 2016, ApJ, 832, 1
Mandelbaum R., Seljak U., Cool R. J., Blanton M., Hirata C. M., Brinkmann J., 2006, MNRAS, 372, 758
Mandelbaum R., Wang W., Zu Y., White S., Henriques B., More S., 2016, MNRAS, 457, 3200
Mao Y.-Y., Zentner A. R., Wechsler R. H., 2018, MNRAS, 474, 5143
Marinacci F. et al., 2018, MNRAS, 480, 5113
Matthee J., Schaye J., 2019, MNRAS, 484, 915
Meng J., Li C., Mo H., Chen Y., Wang K., 2020,arXiv:2008.13733 [astro-ph]
Mo H. J., White S. D. M., 1996, MNRAS, 282, 347
Mo H., Van den Bosch F., White S., 2010, Galaxy Formation and Evolution. Cambridge Univ. Press, Cambridge
More S., van den Bosch F. C., Cacciato M., Skibba R., Mo H. J., Yang X., 2011, MNRAS, 410, 210
Moster B. P., Naab T., White S. D. M., 2013, MNRAS, 428, 3121
Moster B. P., Naab T., White S. D. M., 2018, MNRAS, 477, 1822
Moustakas J. et al., 2013, ApJ, 767, 50
Nadler E. O. et al., 2023, ApJ, 945, 159
Naiman J. P. et al., 2018, MNRAS, 477, 1206
Navarro J. F., Frenk C. S., White S. D. M., 1997, ApJ, 490, 493
Nelson D. et al., 2018, MNRAS, 475, 624
Nelson D. et al., 2019, Comput. Astrophys. Cosmol., 6, 2
Noll S., Burgarella D., Giovannoli E., Buat V., Marcillac D., Muñoz-Mateos J. C., 2009, A&A., 507, 1793
Pillepich A. et al., 2018a, MNRAS, 473, 4077
Pillepich A. et al., 2018b, MNRAS, 475, 648
Planck Collaboration et al., 2016, A&A, 594, A13
Posti L., Fall S. M., 2021, A&A, 649, A119
Posti L., Fraternali F., Marasco A., 2019, A&A, 626, A56
Pozzetti L. et al., 2010, A&A, 523, A13
Reddick R. M., Wechsler R. H., Tinker J. L., Behroozi P. S., 2013, ApJ, 771, 30
Rodriguez-Gomez V. et al., 2015, MNRAS, 449, 49
Salim S. et al., 2016, ApJS, 227, 2
Salim S., Boquien M., Lee J. C., 2018, ApJ, 859, 11
Schaye J. et al., 2015, MNRAS, 446, 521
Somerville R. S., Primack J. R., 1999, MNRAS, 310, 1087
Springel V., White S. D. M., Tormen G., Kauffmann G., 2001, MNRAS, 328, 726
Springel V. et al., 2018, MNRAS, 475, 676
Tojeiro R. et al., 2017, MNRAS, 470, 3720
Vale A., Ostriker J. P., 2004, MNRAS, 353, 189
Vogelsberger M., Genel S., Sijacki D., Torrey P., Springel V., Hernquist L., 2013, MNRAS, 436, 3031
Wang H., Mo H. J., Jing Y. P., Yang X., Wang Y., 2011, MNRAS, 413, 1973
Wang H., Mo H. J., Yang X., Jing Y. P., Lin W. P., 2014, ApJ, 794, 94
Wang H. et al., 2016, ApJ, 831, 164
Wang K. et al., 2019, MNRAS, 488, 3541
Wang K., Mo H. J., Li C., Meng J., Chen Y., 2020, MNRAS, 499, 89
Wang K., Mao Y.-Y., Zentner A. R., Guo H., Lange J. U., van den Bosch F. C., Mezini L., 2022, MNRAS, 516, 4003
Wang K., Peng Y., Chen Y., 2023a, MNRAS, preprint (arXiv:2304.06886)
Wang K., Mo H., Li C., Chen Y., 2023b, MNRAS, 520, 1774
Watson D. F. et al., 2015, MNRAS, 446, 651
Wechsler R. H., Tinker J. L., 2018, ARA&A, 56, 435
Wechsler R. H., Bullock J. S., Primack J. R., Kravtsov A. V., Dekel A., 2002, ApJ, 568, 52
Wechsler R. H., Zentner A. R., Bullock J. S., Kravtsov A. V., Allgood B., 2006, ApJ, 652, 71
Weinberger R. et al., 2017, MNRAS, 465, 3291
White S. D. M., Frenk C. S., 1991, ApJ, 379, 52
White S. D. M., Rees M. J., 1978, MNRAS, 183, 341
Woo J. et al., 2013, MNRAS, 428, 3306
Wright R. J., Lagos C. d. P., Power C., Correa C. A., 2021, MNRAS, 504, 5702
Yang X., Mo H. J., van den Bosch F. C., 2003, MNRAS, 339, 1057
Yang X., Mo H. J., van den Bosch F. C., Jing Y. P., 2005, MNRAS, 356, 1293
Yang X., Mo H. J., van den Bosch F. C., Pasquali A., Li C., Barden M., 2007, ApJ, 671, 153
Yang X. et al., 2021, ApJ, 909, 143
York D. G. et al., 2000, AJ, 120, 1579
Zentner A. R., Hearin A. P., van den Bosch F. C., 2014, MNRAS, 443, 3044
Zentner A. R., Hearin A., van den Bosch F. C., Lange J. U., Villarreal A. S., 2019, MNRAS, 485, 1196
Zhang Y., Yang X., Guo H., 2021, MNRAS, 507, 5320
Zhang Z., Wang H., Luo W., Zhang J., Mo H. J., Jing Y., Yang X., Li H., 2022, A&A, 663, A85
Zheng Z. et al., 2005, ApJ, 633, 791
Zu Y. et al., 2021, MNRAS, 505, 5117
van de Voort F., Schaye J., Booth C. M., Haas M. R., Dalla Vecchia C., 2011, MNRAS, 414, 2458

APPENDIX A: THE CENTRAL SMHMR-HALO FORMATION TIME RELATION IN THE EAGLE SIMULATION

Here, we show the central SMHMR-halo formation time relation in the EAGLE simulation (Schaye et al. 2015). In this paper, we use the simulation identified as `Ref-L0100N1504`, which contains 2×1504^3 particles in a $(100\mathrm{cMpc})^3$ box. The gas particle mass and the stellar particle mass are 1.81×10^6 $\mathrm{M}_\odot$ and 9.70×10^6 $\mathrm{M}_\odot$, respectively. The simulation adopted a flat ΛCDM cosmology from the *Planck* mission (Collaboration et al. 2014), and the cosmological parameters are $\Omega_\mathrm{m} = 0.307$, $\Omega_\Lambda = 0.693$, $\Omega_\mathrm{b} = 0.04825$, $\sigma_8 = 0.8288$, and $h = 0.6777$. The halo formation time is defined in the same way as in the TNG simulation. The stellar mass we use is the sum of all stellar particles within 30 physical kpc.

Fig. A1 shows the relation between central SMHMRs and halo formation time for TNG and EAGLE. One can see that both models predict that early formed haloes have higher central SMHMRs than their late-formed counterparts and vice versa. The discrepancy between these two models is due to the difference in their stellar mass definition and the implementations of subgrid physics. It is noteworthy to point out that our results have also been tested on `Model-C`, which is totally empirical.

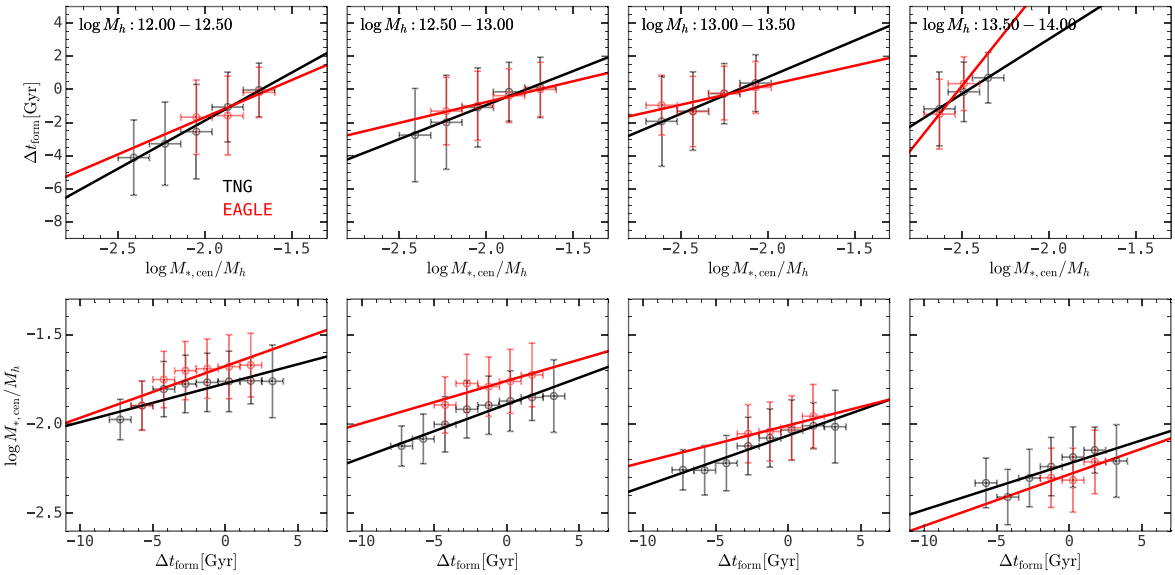

Figure A1. The central SMHMR-halo formation time relation for TNG (black) and EAGLE (red), where the halo mass is recalibrated using the abundance-matching method according to the rank of the total stellar mass in each main halo.

APPENDIX B: DEPENDENCE OF CENTRAL GALAXY PROPERTIES ON CENTRAL SMHMR IN FINE HALO MASS BINS

The quiescent fraction and the spiral fraction of central galaxies in Fig. 5 are in broad halo mass bins with 0.5 dex width for better statistics. Here, Figs B1 and B2 show the results in finer halo mass bins with 0.1 dex width, and one can see that the dependence of the quiescent fraction and the spiral fraction on central SMHMRs is consistent with Fig. 5.

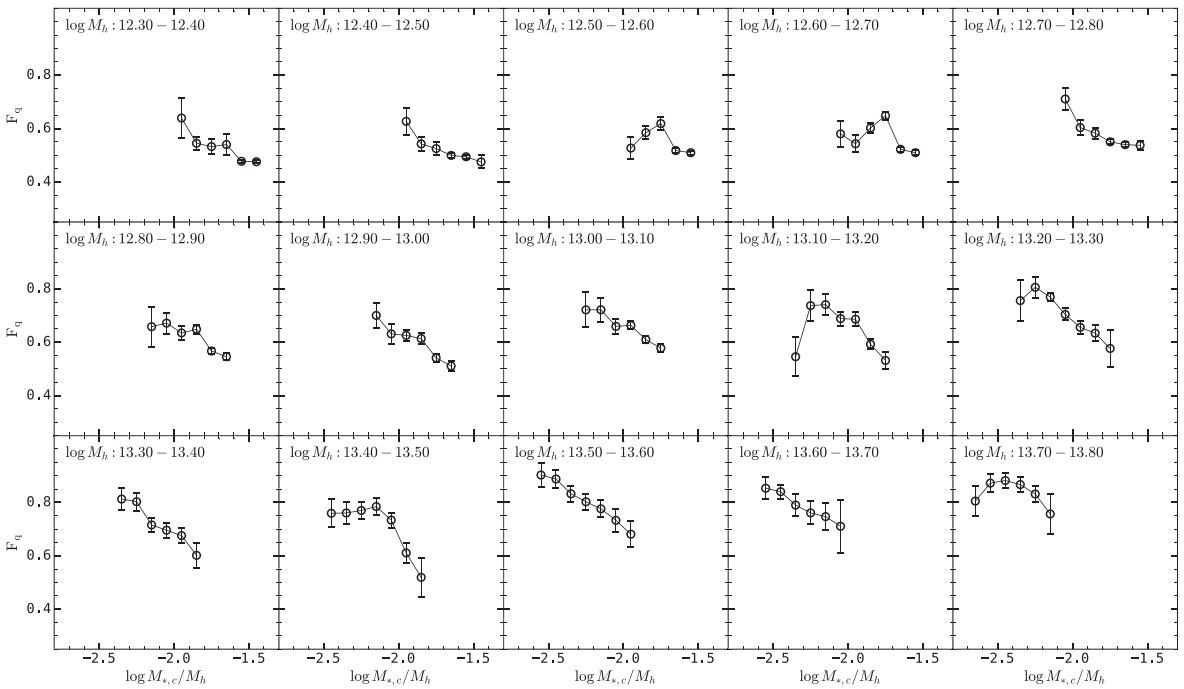

Figure B1. Similar to the top panels of Fig. 5, just in finer halo mass bins.

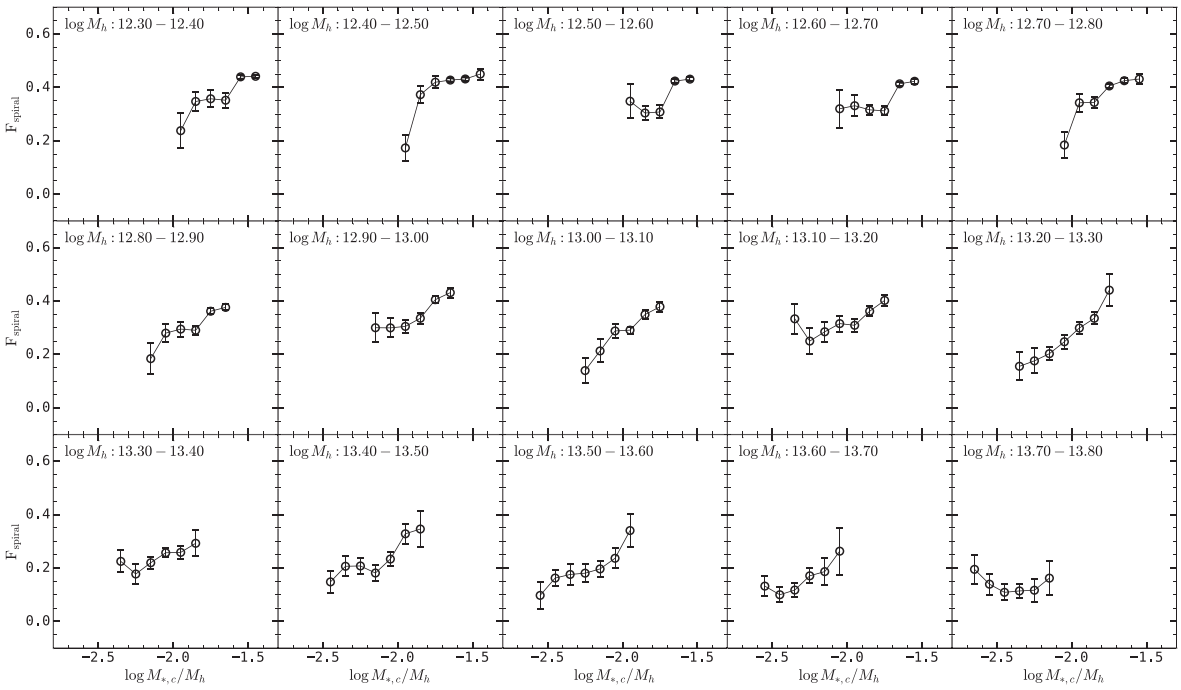

Figure B2. Similar to the bottom panels of Fig. B2, just in finer halo mass bins.

APPENDIX C: DEPENDENCE OF HALO FORMATION TIME ON CENTRAL GALAXY PROPERTIES

In Section 3.2, we showed that late-formed haloes prefer to host quiescent and non-spiral central galaxies. The correlation between the halo formation time and the central galaxy properties can also be demonstrated by examining if the quiescent and non-spiral central galaxies prefer to live in late-formed haloes. Top panels in Fig. C1 show the median SMHMR for quiescent/star-forming and non-spiral/spiral central galaxies with errors estimated using the bootstrap method. Here, one can see that more massive haloes have lower central SMHMR, and the central SMHMR only has a minor dependence on the properties of central galaxies. Nevertheless, one can still see that star-forming/spiral central galaxies tend to have higher central SMHMRs than those quiescent/non-spiral ones. This result is consistent with previous studies where they found that massive star-forming galaxies have higher central SMHMR (Zhang et al. 2022), and massive spiral galaxies also have higher central SMHMR (Posti et al. 2019).

Here, we can convert the central SMHMR to the halo formation time using the linear fitting functions shown in Fig. 2 and infer the difference in the halo formation time for haloes with different central galaxy properties. The results are shown on the bottom panels of Fig. C1, where one can see that massive haloes with star-forming or spiral-like central galaxies are formed early by $\lesssim$0.4 Gyr. We note that the halo formation time difference between star-forming/spiral and quiescent/non-spiral central galaxies is underestimated here for two reasons. First, from Fig. 3, one can see that the correlation between the central SMHMR and the halo formation time is stronger for `Model-A`, which means that our heuristic abundance-matching method missed some correlation between these two quantities. Secondly, due to the observational limits, some low-mass haloes in observation only have one member galaxy, which produces no difference in their calibrated halo mass.

We note that Correa & Schaye (2020) also inspect the dependence of central galaxy properties on the central SMHMR, where they find that blue/disc central galaxies are more massive than their red/elliptical counterparts for galaxy groups with halo mass less than 10^{13} $M_\odot$. However, they find that this signal disappears once a different stellar mass estimation method is adopted. Here, we want to emphasize that this is due to the inconsistent stellar mass estimators used to calculate central stellar mass and halo mass. In the group catalog of Yang et al. (2007), the halo mass for each galaxy group is estimated by rank-matching the total stellar mass of galaxy groups and the theoretical halo mass distribution, where the stellar mass for each galaxy is estimated using the method in Bell et al. (2003). Consequently, central SMHMRs are equivalent to the central stellar mass to total stellar mass ratios, and if we use different stellar mass estimators to calculate the central stellar mass and the total stellar mass, we may introduce artificial biases.

This effect is demonstrated in Fig. C2. On the left-hand panels, we are showing the central SMHMR as a function of halo mass from the native galaxy group catalog of Yang et al. (2007), where the central stellar mass comes from the GSWLC catalog and the halo mass is from the total stellar mass estimated in Bell et al. (2003). Here one can see that star-forming/spiral galaxies are more massive than their quiescent/non-spiral counterparts, which is similar to the result in Correa & Schaye (2020). The right-hand panels show the result where the halo mass is recalibrated according to equation (3), and both the numerator and the denominator for the central SMHMR are using consistent stellar mass definition. And one can see that the difference disappears for haloes that mass below 10^{13} $M_\odot$, and there is still some difference for haloes with mass above 10^{13} $M_\odot$, as shown in Fig. C1.

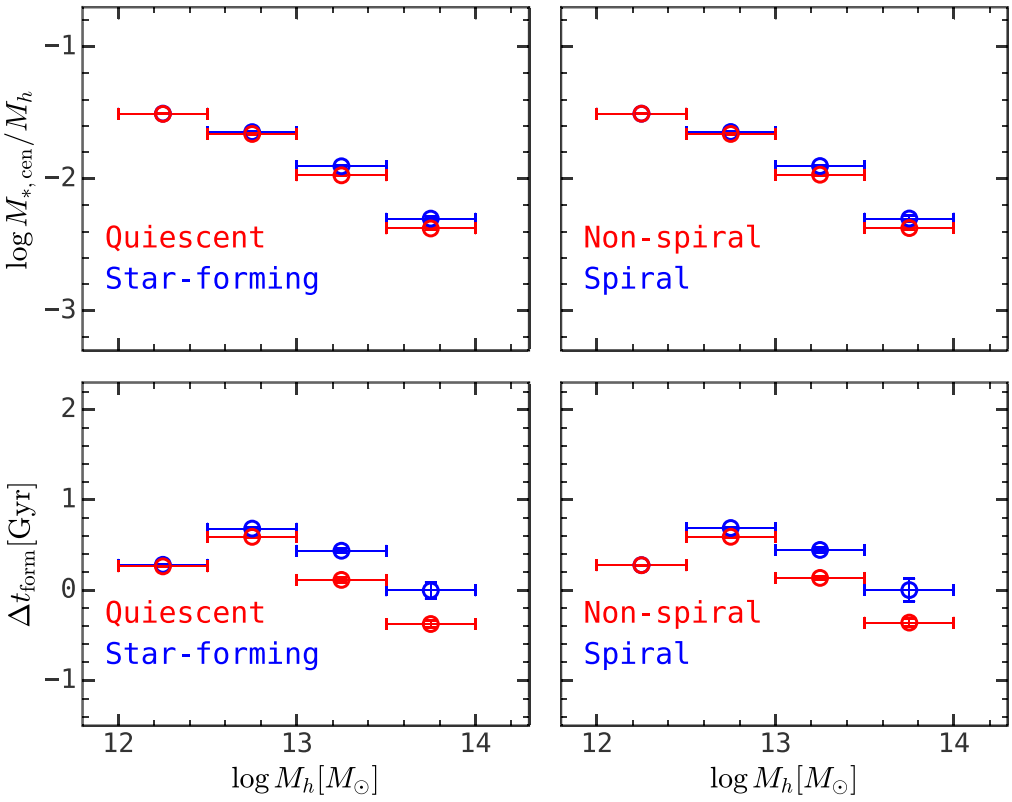

Figure C1. Top panels: Median central SMHMR as a function of halo mass for quiescent/star-forming central galaxies (**left**) and spiral/non-spiral central galaxies (**right**). **Bottom panels:** Median Δt_{form} as a function of halo mass for quiescent/star-forming central galaxies (**left**) and spiral/non-spiral central galaxies (**right**). All error bars are estimated using the bootstrap method.

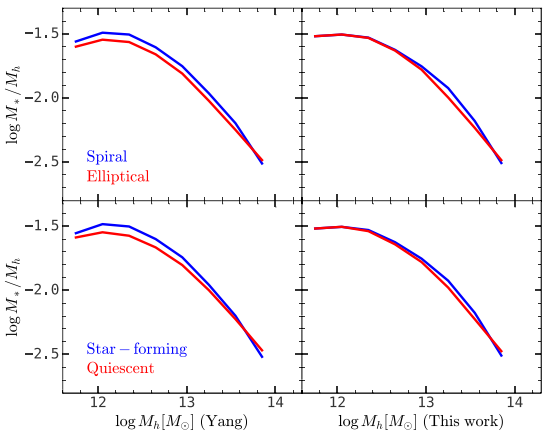

Figure C2. Relation between central SMHMRs and halo masses. **Top panels** show the results for spiral and elliptical galaxies in blue and red colours, respectively. **Bottom panels** show the results for star-forming and quiescent central galaxies, respectively. **Left-hand panels** uses the halo mass calibrated in Yang et al. (2007) group catalog with the rank of the total stellar mass of group members where the stellar mass is estimated from r-band magnitude and $g - r$ colour (Bell et al. 2003). **Right-hand panels** also use the halo mass calibrated according to the rank of total stellar mass, but the stellar mass comes from the GSWLC catalog (Salim et al. 2018). We note that the stellar mass on the y-axis is from the GSWLC catalog.

This paper has been typeset from a TEX/LATEX file prepared by the author.